Please Read the Abstract

By

Abstract Writer

Submitted to the Department of People who read Abstracts and the
Graduate Faculty of the University of Kansas
in partial fulfillment of the requirements for the degree of
Doctor of Philosophy

MEMBER 1, Chairperson

Committee members

MEMBER 2

MEMBER 3

MEMBER 4

Date defended: October 02, 2012

The Dissertation Committee for Abstract Writer certifies
that this is the approved version of the following dissertation :

Please Read the Abstract

MEMBER 1, Chairperson

Date approved: October 03, 2012

Abstract

The first is some LaTeX code, don't change it.

Acknowledgements

I would like to thank all of the little people who made this thesis possible.

Contents

List of Figures

List of Tables

Chapter 1

Introduction

1.1 Theoretical Context

1.2 History

Chapter 2

Theory

2.1 Introduction

Microseconds after the big bang, the universe existed in a state known as the Quark Gluon Plasma (QGP). In the QGP, quarks and gluons are not in hadronic bondage, forced to the confines of bound states such as protons and neutrons. The Large Hadron Collider (LHC) produces QGP in the lab in PbPb (lead-lead) collisions. The high energies and rates of the collisions at the LHC make it possible to do detailed studies of the QGP. The LHC is producing rare experimental probes such as suppressed jets and heavy quarkonia at an unprecedented rate. Physicists now have better constraints on the properties like temperature, viscosity, and energy density of the QGP.

The detailed studies of PbPb collisions coming out of the LHC experiments require an understanding of the initial state of the ions before they collide. Without knowledge of the initial state, physicists cannot determine which experimental effects are due to the QGP and which effects are inherent to the nuclei themselves. For example, suppression of heavy quarkonia is a signature of the QGP but also appears to occur in deuterium-gold collisions where the QGP is not expected to arise [1]. Because it is not certain how much of the reduction of quarkonia production is due to the initial state of the nuclei, the reduction due to the QGP is unclear. Without a clean probe of the initial state, physicists' knowledge of the QGP is limited. Ultra-Peripheral Collisions (UPC) at the

LHC fill this need for a clean probe.

The colliding nuclei interact electromagnetically in an UPC event, avoiding the confusion of nuclear collisions. In UPC events, no QGP state emerges, and the effects arising from the QGP no longer obscure the initial state effects. Other initial state probes such as peripheral nuclear collisions and proton-nucleus collisions have the potential to create the QGP obscuring which effects come from the initial state. It is impossible to create the QGP in UPC events because the nucleons within the nucleus do not collide. UPC events provide clarity by enhancing physicists' understanding of the initial state. UPC events are a probe of the nuclei before they collide that is uncontaminated by QGP effects.

The interactions between the field of photons surrounding the colliding nuclei and the gluons of nuclei can produce a J/Ψ probing the gluon density. The UPC J/Ψ photoproduction cross section is therefore a probe of the the initial state of the nucleus. The Weizsacker-Williams approximation provides a way to calculate the density of probing photons that surrounds the nucleus. The electron-proton scattering data gives a value for the proton photoproduction cross section at lower energies. The perterbutive Quantum Chromodynamics (pQCD), Vector Messon Dominance (VMD), and Leading Twist (LTA) methods all combined the nuclear photon flux with the proton scattering data to calculate the nuclear photoproduction cross section. Each of these methods handle the gluon density of the nucleus differently producing a measurable difference in the value of the J/Ψ photoproduction cross section.

2.2 QCD/QGP

2.3 CGC/intial state

2.4 Weizacker Williams Approximation

The Weizacker-Williams approximation relates the electric field of a stationary point charge to the photon field that arises at ultra relativistic velocities. The approximation is semi-classical and combines both classical and quantum elements. A Fourier transform of Maxwell's equations combine with Einstein's equation for the energy of a photon in the Weizacker-Williams approximation. The frequency modes of the electrostatic field are treated as photons. The conversion of the electric field to a flux of photons simplifies the calculation of interaction cross sections. The Weizsacker-Williams approximation makes the calculation of electromagnetic interactions with the nucleus tractable.

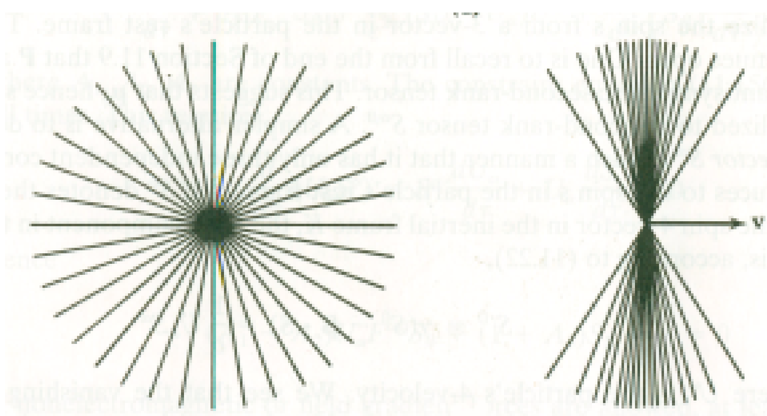

Figure 2.1: The electromagnetic field boosted and at rest.

The Wiezacker-Williams approximation begins with the equation for the electric field of the projectile nucleus at rest. The electromagnetic field only needs to be considered at the position of the target nucleus. From the projectile's point of view, the target is moving and contributes $-vt$ to

Eq. 2.1, the equation for the electric field of the projectile nucleus at rest.

$$x' = -vt' \qquad y' = b \qquad z' = 0 \qquad \vec{\mathbf{E}}' = \left(\frac{eZ}{4\pi\varepsilon_0 \left((-vt')^2 + b^2 \right)^{3/2}} \right) \left(-vt'\hat{\mathbf{x}}' + b\hat{\mathbf{y}}' \right) \tag{2.1}$$

In Eq. 2.1, b is the impact parameter, the distance of separation at closest approach, v is the velocity of the projectile nucleus, Z is the number of protons in the nucleus, and e is the charge of the electron. Two simplifications occur due to the coordinates of Eq. 2.1. The magnetic field is equal to zero, because the projectile is at rest, and the z coordinate can be ignored, reducing the equation to two dimensions.

The Lorentz transformation converts the field equations in the projectile's frame to equations in the target's frame. The result is a set of equations that relate the electric and magnetic field components in one frame to the components of the electric and magnetic field in another frame moving at a different constant velocity. Eq. 2.2 gives the result of the transformation from the projectile's primed frame to the target's rest frame for the field components [2]:

$$\begin{aligned} E'_x = E_x \qquad \gamma\left(E'_y/c + \beta B'_z\right) = E_y/c \qquad \gamma\left(E'_z/c = \beta B'_y\right) = E_z/c \\ B'_x = B_x \qquad \gamma\left(B'_y - \beta E'_z/c\right) = B_y \qquad \gamma\left(B'_z + \beta E'_y/c\right) = B_z \end{aligned} \tag{2.2}$$

The transformation equations for the fields, Eq. 2.2, and the transformation of the coordinates reduce to Eq. 2.3 [2]:

$$\begin{aligned} E'_x = E_x \qquad \gamma E'_y = E_y \qquad \gamma\beta E'_y/c = B_z \\ ct' = \gamma ct \qquad x' = -\gamma\beta ct \end{aligned} \tag{2.3}$$

The simplicity of Eq. 2.1 creates the simplicity of Eq. 2.2. The Lorentz transformation reduces the six components of the electromagnetic field in the target's frame to the three equations in Eq. 2.2 by relating them to the fields of the projectile's frame.

The combination of Eq. 2.1 and Eq. 2.2 produce equations for the electric and magnetic fields in the target's rest frame. Eq. 2.1 gives the expression for the field components as seen in the projectile frame.

$$\vec{\mathbf{E}} = \left(\frac{\gamma e Z}{4\pi\varepsilon_0 \left((\gamma v t)^2 + b^2 \right)^{3/2}} \right) (vt\hat{\mathbf{x}} + b\hat{\mathbf{y}})$$
$$\vec{\mathbf{B}} = \frac{\gamma\beta e Z b}{4\pi c \varepsilon_0 \left((\gamma v t)^2 + b^2 \right)^{3/2}} \hat{\mathbf{z}} = \frac{\gamma \mu_0 v e Z b}{4\pi \left((\gamma v t)^2 + b^2 \right)^{3/2}} \hat{\mathbf{z}} \tag{2.4}$$

If the impact parameter b goes to zero, the target sits in the line of the projectile particle's motion, and the denominator carries a factor of γ squared. If vt goes to zero, the projectile particle is directly above or below in the y direction, and the numerator carries a factor of γ. This results in fields that are a factor of γ^3 higher in the y direction than in the x direction (see Fig. 2.1). The boost compresses the electric field of the charge in the direction of the boost and produces a magnetic field resulting in a form similar to radiation. The point charge at ultra relativistic velocities produces a strong electric field in the plane transverse to its motion resembling a plane wave.

Separating the even and odd functions of the electromagnetic field simplify the decomposition of the field equations into Fourier modes. The even functions decompose into cosine functions, odd functions into sine functions. The y-component of the electric field and the z-component of the magnetic field are even functions in time, and the x-component of the electric field is an odd function in time. Eq. 2.5 gives the Fourier transformation integrals.

$$E_x(\omega) = \sqrt{\frac{2}{\pi}} \frac{eZ}{4\pi\varepsilon_0 b^2} \int_0^\infty \frac{(\gamma v t/b) \sin(\omega t)}{\left((\gamma v t/b)^2 + 1 \right)^{3/2}} dt \qquad E_y(\omega) = \sqrt{\frac{2}{\pi}} \frac{\gamma e Z}{4\pi\varepsilon_0 b^2} \int_0^\infty \frac{\cos(\omega t)}{\left((\gamma v t/b)^2 + 1 \right)^{3/2}} dt$$
$$B_z(\omega) = \frac{\beta E_y(\omega)}{c} \tag{2.5}$$

With the appropriate substitutions, tables provide solutions to the integrals of Eq. 2.5 as seen in

Ref. [3].

$$u = \frac{\gamma v t}{b} \qquad du\left(\frac{b}{\gamma v}\right) = dt \qquad \omega' = \frac{\omega b}{\gamma v}$$
$$\int_0^\infty \frac{u\sin(\omega' u)}{(u^2+1)^{3/2}}du = \omega' K_0(\omega') \qquad \int_0^\infty \frac{\cos(\omega' u)}{(u^2+1)^{3/2}} = \omega' K_1(\omega') \tag{2.6}$$

The Fourier transformation replaces the time variable with a frequency variable in the field equations. The frequency relates to photon energy by the Einstein's photon energy equation, $E = \hbar\omega$. The substitution of time with frequency allows for a flux of photons to replace the classical electromagnetic field.

The γ dependence of the field components is different because of the different t dependence of Eq. 2.6. The integrals in Eq. 2.6 shift the γ dependence of the field component equations. Eq. 2.7 gives the result of the integrals:

$$E_x(\omega) = \sqrt{\frac{2}{\pi}}\frac{eZ}{4\pi\varepsilon_0 b^2}\frac{b}{\gamma v}\frac{\omega b}{\gamma v}K_0\left(\frac{\omega b}{\gamma v}\right) \qquad E_y(\omega) = \sqrt{\frac{2}{\pi}}\frac{\gamma e Z}{4\pi\varepsilon_0 b^2}\frac{b}{\gamma v}\frac{\omega b}{\gamma v}K_1\left(\frac{\omega b}{\gamma v}\right) \tag{2.7}$$

γ is subsumed into the substitution from t to ω in the numerator of the x-component and becomes a part of the zeroth-order modified Bessel function upon integration. The y-component does not have a factor of t in the numerator, therefore the factor of γ remains outside of the integral, and it does not get subsumed into the first-order modified Bessel function. In Eq. 2.7, E_y carries an additional factor of γ in the numerator relative to the E_x. E_y is γ times larger then E_x.

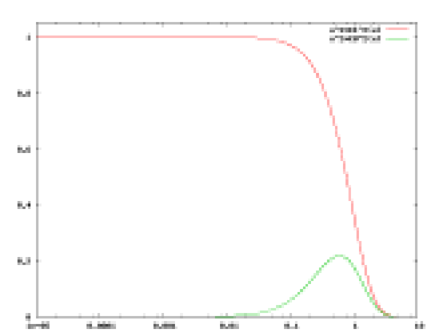

Figure 2.2: The zero and first order modified Bessel functions.

In the ultra-relativistic limit, the electric and magnetic fields have the same configuration as electromagnetic plane wave radiation. The electric and magnetic fields are perpendicular and related by a factor of c in the ultra relativistic limit. When v approaches c, $\beta \approx 1$,

the y-component of the electric field and the z-

component of the magnetic field are related by a factor of c, $E_y/c = B_z$. Because $K_0(x)$ is smaller than $K_1(x)$ for all x, when $\gamma >> 1$, E_y is approximately equally to $\gamma\, E_x$. The conditions imposed by the ultra-relativistic limit result in the relationship of Eq. 2.8.

$$\gamma >> 1 \rightarrow \gamma E_x >> E_x \rightarrow E_y >> E_x \tag{2.8}$$

The x-component of the electric field can therefore be ignored and the magnetic and electric fields are left perpendicular to each other. The six field components reduced to one electric component and one perpendicular magnetic field component, which have a configuration identical to a plane wave.

As with plane waves, the energy per area per time transfered by the electromagnetic field is given by the Poynting vector. The Poynting vector takes the simple form of a plane pulse propagating in the x direction.

$$\vec{\mathbf{S}} \equiv \vec{\mathbf{E}} \times \vec{\mathbf{B}}/\mu_0 = \left(E_y^2/c\mu_0\right)\hat{\mathbf{x}} = c\varepsilon_0 E_y^2 \hat{\mathbf{x}} \tag{2.9}$$

The Poynting vector relates to the fluence (energy per unit area) [4],

$$I(b) = \hat{\mathbf{x}} \cdot \int_0^\infty \vec{\mathbf{S}} d\omega = \int_0^\infty \left(c\varepsilon_0 E_y^2\right) d\omega = \int_0^\infty \left(\frac{dI}{d\omega}\right) d\omega \tag{2.10}$$

and the spectral fluence (energy per area per frequency).

$$\frac{dI}{d\omega} = c\varepsilon_0 E_y^2 = \frac{e^2 Z^2 c}{4\pi^3 b^2 v^2 \varepsilon_0}\left(\frac{\omega b}{\gamma v}\right)^2 K_1^2\left(\frac{\omega b}{\gamma v}\right) = \alpha\hbar\left(\frac{Z}{b\beta\pi}\right)^2\left(\frac{\omega b}{\gamma v}\right)^2 K_1^2\left(\frac{\omega b}{\gamma v}\right) \tag{2.11}$$

Substituting Eq. 2.7 into Eq. 2.10 gives the Poynting vector as a function of frequency. Eq. 2.11 paves the way for Einstein's equation. The spectral fluence given by Eq. 2.11 relates the frequency to energy, which are the same quantities present in Einstein's equation.

Einstein's equation, $E = \hbar\omega$, gives the energy of a photon, which is related to the spectral fluence. If the fluence is due to a photon number density, N, Einstein's equation relates N to the fluence. The relationship between the number of photons per unit area in an infinitesimal energy range and the spectral fluence in an infinitesimal frequency range is given by Eq. 2.12 [2].

$$\frac{dI}{d\omega}d\omega = \hbar\omega N(\omega)d(\hbar\omega) \rightarrow \frac{1}{\hbar^2\omega}\frac{dI}{d\omega} = N(\omega) \tag{2.12}$$

Plugging Eq. 2.11 into Eq. 2.12 yields the semiclassical photon flux of an ultra-relativistic nucleus.

$$N(\omega,b) = \frac{\alpha}{\hbar\omega}\left(\frac{Z}{b\beta\pi}\right)^2\left(\frac{\omega b}{\gamma v}\right)^2 K_1^2\left(\frac{\omega b}{\gamma v}\right) \tag{2.13}$$

Eq. 2.13 replaces the classical electric field of a point charge with a semiclassical field of photons. Physicists can calculate the electromagnetic interactions between nuclei with the final result of the Wiezacker-Willaims approximation, Eq. 2.13. The photon flux in Eq. 2.13 provides the electromagnetic input to the J/Ψ photoproduction cross section calculation.

2.5 Vector Meson Dominance

The Vector Messon Dominace method for calculating the J/Ψ photoproduction cross section has three main components. VMD approach is constructed from the Weizsacker-Williams photon flux, the VMD fit to the proton-electron data, and the Glauber model for calculating the nuclear cross sections from the proton-electron cross sections. The Weizsacker-Williams photon flux provides the probe. The proton-electron scattering data combine with the Glauber model and create a picture of the initial state of the nucleus. Each of the different approaches to calculating the UPC J/Ψ photoproduction cross section use these same elements. However, the different models each use the last two elements differently to produce different pictures of the nucleus and different cross sections values.

The photon flux in the photoproduction cross section calculation must be finite in order for the cross section to be meaningful. The Weizsacker-Williams approximation, Eq. 2.13, produces a divergence at $b = 0$. The probability of the nuclei interacting would exceed one if the photon flux were infinite. The divergence that arises at $b = 0$ from K_1 results in an unphysically infinite photon flux. Removing the divergence is necessary. Special treatment of impact parameter, b, where the colliding nuclei overlap eliminates the divergence.

A modulation of the photon flux can subdue the divergence at $b = 0$. A convolution of the photon flux with the nucleon number density functions of the colliding nuclei produces the necessary modulation. Eq. 2.14 gives the nucleon density of a single nucleus,

$$\rho_A(s) = \frac{\rho_0}{1 + exp[(s - R_{WS})/d)]} \tag{2.14}$$

In Eq. 2.14, s is the distance from the center of the nucleus, R_{WS} is the radius of the nucleus, and d is the skin depth, which determines how quickly the nucleon density falls off beyond the nuclear radius. In Eq. 2.15 the depth of the nucleus is integrated out leaving just the transverse dimension in T_A. The average number of nucleons in the overlap region is given by a convolution of T_A from each of the two nuclei to produce T_{AA}.

$$\begin{aligned} T_A(\vec{r}) &= \int dz \rho_A(\sqrt{|\vec{r}|^2 + z^2}) \\ T_{AA}(|\vec{b}|) &= \int d^2\vec{r} T_A(\vec{r}) T_A(\vec{r} - \vec{b}) \end{aligned} \tag{2.15}$$

T_{AA} is the function that modulates the photon flux. As input to the Poisson distribution, T_{AA} reduces Eq. 2.13 at values of b where the nuclei overlap significantly and eliminates the divergence in the photon flux.

Modulating the photon flux by the probability that no nucleon-nucleon collisions occur limits the photon flux at low b in Eq. 2.13 The convolution of the photon flux with the b dependent probability that no nucleon-nucleon collisions occur removes the divergence in Eq. 2.13. Using the mean number of nucleons in the overlap region given by T_{AA}, the Poisson distribution gives the probability that no collisions occur at a given b:

$$P_0(b) = exp[-T_{AA}(b)\sigma_{NN}] \tag{2.16}$$

In Eq. 2.16, σ_{NN} is the cross section for a nucleon-nucleon interaction, which gives the probability that a collision will occur given the average number of nucleons in the overlap region. The average photon flux over impact parameter, b, can be calculated from the integration of the b-dependent photon flux, Eq. 2.13, with the b-dependent probability of having no nucleon-nucleon interactions, Eq. 2.16.

$$\frac{dN_\gamma(k)}{dk} = \int_0^\infty 2\pi b db P_0(b) \int_0^R \frac{rdr}{\pi R_A^2} \int_0^{2\pi} d\phi \frac{d^3N_\gamma(k, b + r\cos(\phi))}{dkd^2r} \tag{2.17}$$

Eq. 2.17 goes down to $b = 0$ where the photon flux is infinite, but because the probability of having a nucleon-nucleon collisions is high, the divergence is eliminated. The result of Eq. 2.17 does not diverge.

A power-law fit to the proton photoproduction data gives an analytic expression for the energy dependence of the proton photoproduction cross section. The fitting function is simple and only depends on the photon-proton center of mass energy, W. Eq. 2.18 gives the parameterization of the forward proton photoproduction cross section fit.

$$\left.\frac{d\sigma(\gamma p \rightarrow Vp)}{dt}\right|_{t=0} = b_v(XW^\varepsilon + YW^{-\eta}) \tag{2.18}$$

W is the center of mass energy of the proton-photon system in Eq. 2.18. The remaining variables in Eq. 2.18 are simply powerlaw-fit parameters. The XW^ε term characterizes pomeron mediated interactions, and the YW^η term characterizes meson mediated interactions[5]. J/Ψ's high mass relative to the π and ρ renders the second term in Eq. 2.18 negligible as the term falls rapidly with increasing W. Eq. 2.18 allows for extrapolation and interpolation of the measured forward proton photoproduction cross section. The fit to the data provides estimates for energies that have not yet been probed experimentally.

The proton-electron scattering data is used differently in the VMD method than in the other major methods. The VMD method for calculating UPC photoproduction cross sections relies more on electron-proton scattering data. The proton photoproduction cross sections from the electron-proton scattering data is a direct input to the VMD model. A power-law fit to the proton photoproduction data, as opposed to model dependent gluon densities of other approaches, combines with the Glauber model to provide the nuclear model in the VMD method. Because of the simplicity of the method, the VMD approach incorporates less modifications of the nuclear initial state relative to the proton initial state. As a result, the VMD method produces a higher UPC J/Ψ photoproduction cross section relative to the other methods.

Vector meson dominance and the optical theorem allow for the calculation of the total proton-meson scattering cross section from the fit given by Eq. 2.18. The optical theorem relates a total cross section, σ, to a corresponding forward scattering cross section, $d\sigma/dt|_{t=0}$. Vector meson dominance asserts that the colored part of the photon wave function is dominated by vector mesons; therefore, the photon is represented as a quark-antiquark pair in photoproduction calculations. These two components combine to produce Eq. 2.19.

$$\begin{aligned} \frac{d\sigma(\gamma p \to Vp)}{dt}\Big|_{t=0} &= \frac{4\pi\alpha}{f_v^2(M_V,\Gamma_{l^+l^-})}\frac{d\sigma(Vp \to Vp)}{dt}\Big|_{t=0} \\ \sigma(Vp)^2_{tot} &= 16\pi\frac{d\sigma(Vp \to Vp)}{dt}\Big|_{t=0} \end{aligned} \tag{2.19}$$

In Eq. 2.19, the photon-proton scattering is related to meson-proton scattering through the photon-meson coupling, which depends on the vector meson's mass, M_V, and leptonic decay width, $\Gamma_{l^+l^-}$. The result of combining vector meson dominance and the optical theorem in Eq.2.19 provides the cross section for a meson to scatter off a proton. The total proton-meson scattering cross section, provides the input to the Glauber model calculation of the nuclear photoproduction cross section.

The nucleus-meson scattering cross section relates to Eq. 2.19 through the Glauber model. The Glauber model allows for Eq. 2.19, the proton-meson scattering cross section, to be used to calculate a nucleus-meson scattering cross section. The Glauber model produces nuclear cross section calculations from nucleon (proton or neutron) interaction cross sections by use of T_{AA}. The combination of the mean number of nucleons in the overlapping region of a nucleus-nucleus collision, T_{AA}, the nucleon cross section, σ, and the Poisson distribution make-up the core of the Glauber model. For the total nucleus-meson scattering cross section, the equation has the following form:

$$\sigma_{tot}(VA) = \int d^2\vec{r}(1 - e^{-\sigma_{tot}(Vp)T_{AA}(\vec{r})}) \tag{2.20}$$

In Eq. 2.20, the term $e^{\sigma_{tot}(Vp)T_{AA}}$ gives the probability of having no meson-nucleon scatterings from the Poisson distribution. The probability of having at least one scattering is given by subtracting one from the term $e^{\sigma_{tot}(Vp)T_{AA}}$ in Eq. 2.20. As seen in Eq. 2.20, the Glabuer model leverages scientific knowledge of the proton to understand of the nucleus. The Glauber model is the tool that combines the proton photoproduction data with nucleon distributions in the nucleus to produce a nuclear vector meson photoproduction cross section in the VMD approach.

Reversing the process used for the proton, Eq. 2.20, the meson nucleus scattering cross section, relates to forward nuclear photoproduction cross section through the optical theorem. The nuclear photoproduction cross section is the input to the calculation of the final result, the nuclear vector meson photoproduction cross section in UPC events. Eq. 2.21 uses the optical theorem to produce the nuclear photoproduction cross section from the nucleus-meson scattering cross section:

$$\begin{aligned} \frac{d\sigma(\gamma A \to VA)}{dt}\Big|_{t=0} &= \frac{\alpha\sigma_{tot}^2(VA)}{4\pi f_v^2} \\ \sigma(\gamma A \to VA) = \frac{d\sigma(\gamma A \to VA)}{dt}\Big|_{t=0} &\int_{t_{min}}^{\infty} dt|F(t)|^2 \end{aligned} \tag{2.21}$$

F in equation Eq. 2.21 is the Fourier transform of the nuclear density function, ρ_A. To produce the formula for calculating the UPC vector meson photoproduction cross section, Eq. 2.21 is combined with the photon flux incident on the nucleus, Eq. 2.17.

$$\sigma(AA \to AAV) = 2\int dk \frac{dN_\gamma}{dk}\sigma(\gamma A \to VA) \tag{2.22}$$

The factor of 2 in Eq. 2.22 comes from the fact that both of the two colliding nuclei contribute. Combining the three elements of VMD, Eq. 2.22 is the final result of the VMD UPC photoproduction cross section calculation. Vector meson production rates in UPC collisions are predicted by Eq. 2.22, which can be confirmed or denied by experiment.

2.6 Leading Twist Approach Derivation

The LTA method for calculating UPC photoproduction cross sections combines elements of the Glauber model with direct use of gluon densities. The proton gluon density is modified by a nuclear modification function in the LTA method to produce the nuclear gluon density. The nuclear modification function converts the proton photoproduction cross section to a nuclear photoproduction cross section in the LTA method. The LTA method is different from the other methods in its direct use of the nuclear modification factor and how the nuclear modification factor calculation incorporates multiple scattering. The direct use of the nuclear modification factor produces the most gluon shadowing out of the three major methods, and results in the lowest cross sections. The LTA method is the easiest to constrain experimentally for this reason.

The LTA method uses the Weizacker-Williams approximation to calculate the photon flux created by the colliding nuclei. As in the VMD method, the probability of having no hadronic collisions modulates the flux. The photon flux for the LTA method has the following form [6]:

$$x = \frac{\omega b}{\gamma_L v}$$

$$n^i_{\gamma/A}(\omega_\gamma) = \frac{2\alpha Z^2}{\pi} \int_{b_{min}}^{\infty} db \frac{x^2}{b} \left[K_1^2(x) + \frac{K_0^2(x)}{\gamma_L^2} \right] P_0(b) P_C^i(b) \tag{2.23}$$

The $K_0^2(x)$ term contributes a photon flux in the transverse direction. $P_C^i(b)$ is an additional modulation factor that requires various additional interactions. These interactions result in additional emissions of neutrons from the receding nuclei as the nuclei relax from excited states. The LTA flux reproduces the VMD result when the K_0 term becomes negligible as γ_L approaches ∞ and

$P_C^i = 1$ when all emissions are allowed. The terms P_C^i and K_0 create additional ways to distinguish UPC events from nuclear collisions experimentally but leave the underlying interaction mechanism the same. For example, the additional terms in the LTA formulation of the photon flux produce calculations of asymmetric neutron emission, which separate UPC events from nuclear collisions.

The LTA method calculates the nucleon photoproduction cross section from the nucleon gluon density. Ref. [6] derives the nucleon cross section from derivations of the nucleon gluon densities from electron-proton scattering data and leading order perturbative quantum field theory calculations. The forward photoproduction cross section of the nucleon has the following form [6]:

$$\frac{d\sigma_{\gamma N\to J/\Psi N}(t=0)}{dt} = \frac{16\Gamma_{l^+l^-}\pi^3}{3\alpha M_{J/\Psi}^5}[\alpha_s\mu^2 xG_N(x,\mu^2)]^2 \tag{2.24}$$

Here G_N is the gluon density of the nucleon, x is the fraction of the nucleon's momentum the gluon carries, and μ is related to momentum at which the nucleon is being probed, which is equal to $M_{J/\Psi}/2$ for J/Ψ photoproduction. In Eq. 2.24 the nucleon cross section is explicitly connected to the gluon density. By connecting the gluon density to the cross section, Eq. 2.24 allows for the gluon density to be experimentally probed.

Ref. [6] exploits the optical theorem to relate the forward photoproduction cross section of the nucleon to the nuclear cross section. Eq. 2.25 gives the relation:

$$R_g = \frac{G_A(x,\mu^2)}{AG_N(x,\mu^2)}$$

$$\sigma_{\gamma A\to J/\Psi A}(\omega) = \frac{d\sigma_{\gamma N\to J/\Psi N}}{dt}(\omega,t_{min})R_g^2\int_{t_{min}}^{\infty} dt|F(t)|^2 \tag{2.25}$$

R_g, the nuclear modification function, is the ratio between the gluon density of the nucleon, G_N, to the gluon density of the nucleus, G_A. As with the VMD method, the optical theorem relates the forward cross section, $\frac{d\sigma_{\gamma N\to J/\Psi N}}{dt}(\omega,t_{min})$, to the total cross section, $\sigma_{\gamma A\to J/\Psi A}$. The LTA method relates the measurable UPC photoproduction cross section to the gluon density of the nucleus. Eq. 2.25 further connects the gluon density of the nucleon to the relative reduction of the gluon density in the nucleus through R_g.

From Eq. 2.25, the LTA method can predict the angular distribution of photoproduced J/Ψ with respect to the beam axis. In Ref. [7] the angular distribution is expressed in the form of the rapidity dependency of the UPC photoproduction cross section.

$$\frac{d\sigma_{A_1A_2\to A_1A_2J/\Psi}}{dy} = n_{\gamma/A_1}(y)\sigma_{\gamma A_2\to J/\Psi A_2}(y) + n_{\gamma/A_2}(-y)\sigma_{\gamma A_1\to J/\Psi A_1}(-y) \tag{2.26}$$
$$y = ln\Big(\frac{2\omega}{M_{J/\Psi}}\Big)$$

Eq. 2.26 is comprised of two terms, one for photons from the forward going nucleus interacting with the backward going nucleus, and a second for the reverse situation. The integration of Eq. 2.26 over y produces the factor of 2 that is present in Eq. 2.22. The rapidity distribution of the photoproduction cross section given in Eq. 2.26 provides a more detailed prediction and allows for more direct experimental comparison. Eq. 2.26 allows for comparison to rapidity regions that are covered by experiments.

The LTA method is distinct from the pQCD method and VMD method through the use R_g, the nuclear gluon modification factor. As opposed to using R_g, the pQCD method uses the nuclear gluon density, and VMD model uses proton photoproduction cross sections directly. In the LTA method, R_g is calculated through a combination of J/Ψ photoproduction data from proton-electron scattering and DGLAP evolution equations, which incorporates nuclear multiple scattering effects [6]. The DGLAP evolution equations give the depends of nuclear gluon densities on the momentum scale at which the nucleus is probed, μ in Eq. 2.24. The unique way the LTA method calculates R_g results in lower cross sections than the other major methods and allows for experimental sensitivity. Experimental measurements of the UPC J/Ψ photoprodcution cross section with CMS have the opportunity to distinguish whether R_g as calculated in the LTA method accurately predicts the gluon density of the nucleus.

2.7 Perturbative Quantum Chromodynamics

To calculate the UPC J/Ψ photoproduction cross section, the pQCD method uses the nuclear gluon density to characterize the nucleus and the Wiezacker-Willaims approximation for the probing photon flux. The pQCD method combines these components such that the nuclear gluon density is a direct variable. The direct use of the nuclear gluon density in the pQCD method allows for the use of a variety of nuclear gluon density models. A range of nuclear gluon densities are present in the available models resulting in a wide range of cross section values. The UPC J/Ψ photoproduction cross section is correlated with the gluon density of the nucleus rising with higher densities and shrinking with lower densities. In the pQCD approach, the calculation of the UPC J/Ψ photoproduction cross section allows experiments to constrain many different nuclear gluon density models.

In the pQCD method, the photon interacts with the nucleus by fluctuating to a quark-anitquark pair. For J/Ψ, the photon fluctuates to a $c\bar{c}$ pair. The probability for the photon to fluctuate to a $c\bar{c}$ pair depends on the $M_{J/\Psi}$, the mass of J/Ψ, $\Gamma_{l^+l^-}$, the J/Ψ leptonic decay width, and α, the electromagnetic coupling constant. These three variables connect the c quark to the electromagnetic force mediator, the photon. Recast as a $c\bar{c}$ pair, the photon couples to the nuclear gluon density. Ref. [8] uses the fluctuation of the photon to a $c\bar{c}$ pair as the foundation for calculating the forward J/Ψ photoproduction cross section.

The $c\bar{c}$ pair arising from the photon fluctuation scatters off the gluons of the nucleus. The density of gluons in the nucleus determines how likely and therefore how large the cross section is for the quarks to scatter and form a J/Ψ. The forward scattering cross section is the portion of those scattering events which transfer the minimum amount of momentum between the photon and the nucleus. The forward cross section for J/Ψ photoproduction in the nucleus has the following form [8]:

$$\frac{d\sigma_{\gamma A\to J/\Psi A}}{dt}\Big|_{t=0} = \xi_{J/\Psi}\Big(\frac{16\pi^3\alpha_s^2\Gamma_{l^+l^-}}{3\alpha M_{J/\Psi}^5}\Big)[xG_A(x,\mu^2)]^2 \tag{2.27}$$

In Eq. 2.27, $\xi_{J/\Psi}$ is an experimentally derived correction factor, α_s is the strong coupling constant,

x is the momentum faction of the nucleus the scattering gluons carry, and G_A is the gluon density of the nucleus. Both the c and $\bar{c}$ couple to the gluon density, and the double coupling results in the squared dependence of the cross section on the gluon density in Eq. 2.27. Fitting Eq. 2.27 to proton-electron scattering data sets $\xi_{J/\Psi}$ [8]. The forward scattering cross section given by Eq. 2.27 connects the photon flux to the gluon density and provides the input to calculate the total cross section by the optical theorem. Eq. 2.27 is the crux of how UPC measurements provide insight into the gluon content of the nucleus.

The optical theorem relates the forward cross section in Eq. 2.27 to the total photoproduction cross section. The total cross section calculated by use of the optical theorem gives the probability that a photon incident on the nucleus will produce a J/Ψ regardless of the momentum transfered in the interaction. Ref. [8] gives the form of the total cross section equation:

$$\sigma_{\gamma A\to J/\Psi A}(k) = \frac{d\sigma_{\gamma A\to J/\Psi A}}{dt}\bigg|_{t=0} \int_{t_{min}(k)}^{\infty} dt |F(t)|^2 \tag{2.28}$$

Here $t_{min} = (M^2_{J/\Psi}/4k\gamma_L)^2$, which is the minimum amount of momentum transfer required to produce a J/Ψ given the photon wave number k. The k dependence of t_{min} produces the rapidity, y, dependence of the total cross section. The total cross section for photoprduction, Eq. 2.28, provides the input to Eq. 2.26, which gives the rapidity dependence of the UPC photoproduction cross section. Eq. 2.28 as input to Eq. 2.26 allows for experimental comparison of the pQCD method to measurements of UPC photoproduction cross sections. With the pQCD method's direct use of the nuclear gluon density in Eq. 2.27, the pQCD method allows for experimental exploration of any gluon density model.

2.8 Incoherent Photoproduction

2.9 Photon Induced Nuclear Break-up

2.10 Theoretical Results

The UPC photoproduction cross section calculations depend significantly on how the nucleus is represented in the calculation. The results from the VMD, LTA, and pQCD methods vary from a relatively large cross section in the VMD model, ranging through a variety of values in the pQCD method, to a relatively small cross section in the LTA method. Each of these methods utilizes the same probe of the nucleus, the equivalent photon flux that is calculated using the Weizsacker-Williams approximation. The three methods deviate in how they calculate the forward photo-production scattering cross section. The differences in the UPC photoproduction cross sections predicted by the different models demonstrates the amount of experimental sensitivity there is to distinguishing between the models. The dependence of the cross section on rapidity shows where in phase space a measurement of the cross section is most sensitive.

The predicted value for the UPC J/Ψ photoproduction cross section in PbPb collisions at the LHC differ widely depending on which of the three main methods is used. The cross section value calculated by Eq. 2.22 in the VMD, LTA, and the various gluon density models in pQCD method vary significantly. Table 2.1 gives the predicted values for the three main methods taken from Ref [9], Ref [6], and Ref [5]. The cross sections in Table 2.1 differ by a factor of ≈ 4 from the smallest to largest and create an experimental opportunity. The clear discrepancy between the models in Table 2.1 demonstrates the high amount of experimental sensitivity there is for distinguishing between the models.

The rapidity dependence of the cross sections determine which values of rapidity will be most sensitive to differences in the models. The rapidity dependence calculated by Eq. 2.26 overlap between the models at certain values of y leaving the models indistinguishable at that rapidity. Fig. 2.3 [10] shows the rapidity dependency of the UPC J/Ψ photoproduction cross section for the

Model	$\sigma_{AA\to AAJ/\Psi}(mb)$
VMD/STARlight MC	23
LTA	9
pQCD-MSTW08	34
pQCD-EPS08	7
pQCD-EPS09	14
pQCD-HKN07	23

Table 2.1: $\sigma_{AA\to AAJ/\Psi}(mb)$ the LTA, VMD, pQCD methods. Four different gluon density models are used in the pQCD method. STARlight is a simulation software package that utilizes the VMD model.

three main models including several different gluon density models using the pQCD method. In

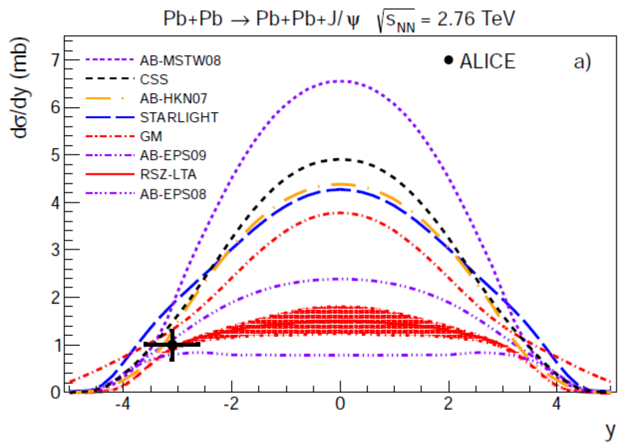

Figure 2.3: AB is the pQCD method, RSZ-LTA is the LTA method, and STARlight is the VMD model.

Fig. 2.3 at higher rapidities, in particular $|y| > 3$, the various models give similar values for $d\sigma/dy$. At $y = 0$ the models vary the most. Fig. 2.3 shows that experiments that can measure J/Ψ at $y = 0$ have the best opportunity to distinguish between the models. The high sensitivity at $y = 0$ creates an advantage for experiments that can measure particles with small rapidity and low momentum.

The UPC photoproduction models each have different shapes to their rapidity dependence. The slope of $d\sigma/dy$ in Fig. 2.3 depends on the model. Through the rapidity region $1 < |y| < 3$, each of the models has a progressively steeper slope. The LTA method and the pQCD method utilizing the EPS08 gluon density model are relatively flat where as the VMD and other gluon density models using the pQCD method have a noticeable slope. The differing slopes provide an additional experimental observable. The shape of the rapidity distributions provide experimental sensitivity at rapidities away from $y = 0$ and creates an opportunity for experiments that can not measure J/Ψ at $y = 0$.

The nuclear suppression factor, S, demonstrates the difference between how the models represent the nucleus. S, which is a ratio between the nuclear photoproduction cross section and the free nucleon photoproduction cross seciton, is a measure of how the nuclear gluon densities evolve in each of the models. Fig. 2.4 from Ref.[11] shows the nuclear suppression, which is equivalent to R_g in Eq. 2.25, for the LTA and pQCD method. Fig. 2.5 shows the nuclear suppression for

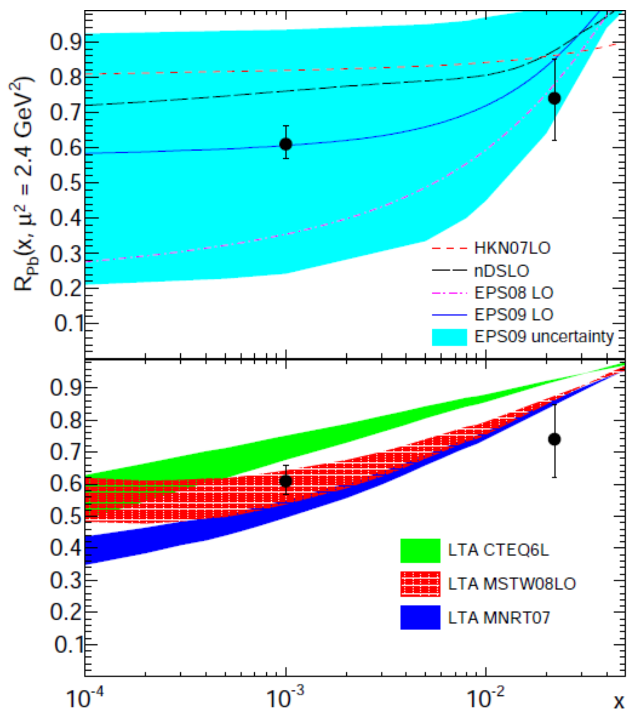

Figure 2.4: Nuclear supression factor, S, in the pQCD and LTA methods.

the VMD method [11]. Fig 2.5 and Fig 2.4 show that as the momentum of the probing photon goes up, increasing $W_{\gamma p}$, and momentum of the probed gluon goes down, decreasing x, the nuclear gluon density decreases relative to the free nucleon. The nuclear suppression factor, S, allows for the different models' representations of the gluon content of the nucleus to be directly compared to each other and to data. S can be measured from data by assuming a Weizacker-Williams photon

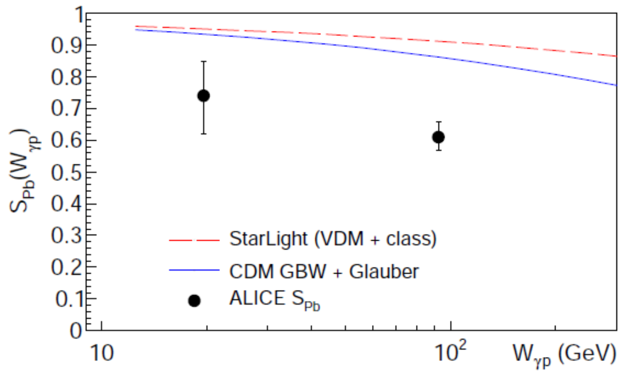

Figure 2.5: Nuclear supression factor, *S*, in VMD method.

flux and provides insight into nuclear gluon densities.

Chapter 3

The CMS Detector

3.1 CMS general

3.2 Muons

3.3 HCal

3.4 ZDC

3.5 Trigger

Chapter 4

Method

4.1 MC Simulation

4.2 Event Selection

4.3 break up determination

4.4 Signal Extraction

4.5 Efficiency determination

Chapter 5

Results

5.1 Coherent cross section

5.2 Incoherent cross section

5.3 Break up ratios

5.4 diMuon-neutron correlations

Chapter 6

Conclusion

6.1 xsection results

6.2 correlation results

Chapter 7

Future Works

7.1 high mass gamma-gamma PbPb 2011

7.2 UPC hadronic overlap PbPb 2011

7.3 pPb J/Psi

7.4 UPC J/Psi 2015

7.5 UPC Upsilon 2015

References

[1] **PHENIX Collaboration** Collaboration, A. Adare *et al.*, "Cold Nuclear Matter Effects on J/ψ Yields as a Function of Rapidity and Nuclear Geometry in Deuteron-Gold Collisions at $\sqrt{s_{NN}} = 200$ GeV," *Phys.Rev.Lett.* **107** (2011) 142301, `arXiv:1010.1246 [nucl-ex]`.

[2] J. D. Jackson, *Classical electrodynamics*. Wiley, New York, NY, 3rd ed. ed., 1999. `http://cdsweb.cern.ch/record/490457`.

[3] E. Fermi, "On the Theory of Collisions between Atoms and Electrically Charged Particles," in *Electromagnetic Probes of Fundamental Physics*, W. Marciano and S. White, eds., pp. 243–252. Sept., 2003. `hep-th/0205086`.

[4] C. A. Brau, *Modern Problems in Classical Electrodynamics*. Oxford, New York, NY, 1st ed. ed., 2004.

[5] S. R. Klein and J. Nystrand, "Exclusive vector meson production in relativistic heavy ion collisions," *Phys. Rev. C* **60** (Jun, 1999) 014903. `http://link.aps.org/doi/10.1103/PhysRevC.60.014903`.

[6] V. Rebyakova, M. Strikman, and M. Zhalov, "Coherent rho and J/psi photoproduction in ultraperipheral processes with electromagnetic dissociation of heavy ions at RHIC and LHC," *Phys.Lett.* **B710** (2012) 647–653, `arXiv:1109.0737 [hep-ph]`.

[7] V. Rebyakova, M. Strikman, and M. Zhalov, "Coherent ρ and J/Ψ photoproduction in ultraperipheral processes with electromagnetic dissociation of heavy ions at RHIC and

LHC," *Physics Letters B* **710** no. 4–5, (2012) 647 – 653.
http://www.sciencedirect.com/science/article/pii/S0370269312003152.

[8] A. Adeluyi and C. A. Bertulani, "Gluon distributions in nuclei probed at energies available at the CERN large hadron collider," *Phys. Rev. C* **84** (Aug, 2011) 024916.
http://link.aps.org/doi/10.1103/PhysRevC.84.024916.

[9] A. Adeluyi and T. Nguyen, "Coherent photoproduction of ψ and Υ mesons in ultraperipheral pPb and PbPb collisions at the CERN Large Hadron Collider at $\sqrt{S_{NN}} = 5$ TeV and $\sqrt{S_{NN}} = 2.76$ TeV," *Phys. Rev. C* **87** (Feb, 2013) 027901, arXiv:1302.4288 [nucl-th]. http://link.aps.org/doi/10.1103/PhysRevC.87.027901.

[10] **ALICE** Collaboration, B. Abelev *et al.*, "Coherent J/ψ photoproduction in ultra-peripheral Pb-Pb collisions at $\sqrt{s_{NN}} = 2.76$ TeV," *Physics Letters B* **718** no. 4–5, (2013) 1273 – 1283.
http://www.sciencedirect.com/science/article/pii/S0370269312012257.

[11] V. Guzey, E. Kryshen, M. Strikman, and M. Zhalov, "Evidence for nuclear gluon shadowing from the ALICE measurements of pbpb ultraperipheral exclusive production," *Physics Letters B* **726** no. 1–3, (2013) 290 – 295.
http://www.sciencedirect.com/science/article/pii/S0370269313006825.

Appendix A

My Appendix, Next to my Spleen

There could be lots of stuff here